Redox transfer at subduction zones: insights from Fe isotopes in the Mariana forearc

Baptiste Debret, C D J Reekie, N Mattielli, H Beunon, B Ménez, I P Savov, H M Williams

Geochemical Perspectives Letters

Redox transfer at subduction zones: insights from Fe isotopes in the Mariana forearc

B. Debret[1*], C.D.J. Reekie[2], N. Mattielli[3], H. Beunon[3], B. Ménez[1], I.P. Savov[4], H.M. Williams[2]

doi: 10.7185/geochemlet.2003

Abstract

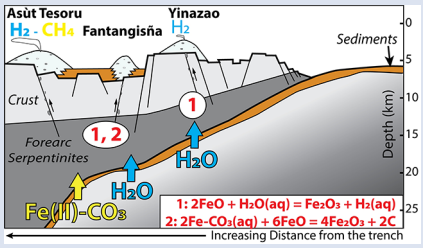

Subduction zones are active sites of chemical exchange between the Earth's surface and deep interior and play a fundamental role in regulating planet habitability. However, the mechanisms by which redox sensitive elements (*e.g.*, iron, carbon and sulfur) are cycled during subduction remains unclear. Here we use Fe stable isotopes (δ^{56}Fe), which are sensitive to redox-related processes, to examine forearc serpentinite clasts recovered from deep sea drilling of mud volcanoes formed above the Mariana subduction zone in the Western Pacific. We show that serpentinisation of the forearc by slab-derived fluids produces dramatic δ^{56}Fe variation. Unexpected negative correlations between serpentinite bulk δ^{56}Fe, fluid-mobile element concentrations (*e.g.*, B, As) and $Fe^{3+}/\Sigma Fe$ suggest a concomitant oxidation of the mantle wedge through the transfer of isotopically light iron by slab-derived fluids. This process must reflect the transfer of either sulfate- or carbonate-bearing fluids that preferentially complex isotopically light Fe.

Received 15 August 2019 | Accepted 10 December 2019 | Published 31 January 2020

Introduction

Subduction zones regulate chemical exchange between the Earth's surface and interior, modulating the long term cycling of redox sensitive elements such as iron, carbon and sulfur (Evans, 2012). Recent iron isotope studies (δ^{56}Fe) have shown that iron, which was previously considered to be insoluble, can be mobilised in slab-derived fluids by complexation with chloride and/or oxidising ligands (*e.g.*, Fe(II)-CO_3 or Fe(II)-SO_4; Debret *et al.*, 2016, 2018). Importantly, these complexes preferentially concentrate light (low) δ^{56}Fe, driving stable isotope fractionation (Debret *et al.*, 2016, 2018). These findings concur with the high $Fe^{3+}/\Sigma Fe$ (Kelley and Cottrell, 2009) and light δ^{56}Fe (Nebel *et al.*, 2015) of arc lavas relative to mid-ocean ridge basalts, although the origin of light δ^{56}Fe in arc lavas remains an active research frontier. Iron stable isotopes are therefore a potentially powerful tool to track the mobility of iron and the fate of oxidised fluids across subduction zones. However, questions remain as to whether iron is sufficiently concentrated in slab-derived fluids to influence the δ^{56}Fe of the sub-arc mantle and if so, do links between the oxidation state and the δ^{56}Fe of mantle wedge peridotites exist?

The transfer of redox sensitive elements across subduction zones involves complex and multi-stage processes (Nebel *et al.*, 2015). For example, both the oxidation state and isotope signature of mantle wedge peridotites are likely to be influenced by existing heterogeneities prior to subduction (Williams *et al.*, 2004), as well as by later metasomatism by slab-derived fluids and/or melts (Huang *et al.*, 2019) and/or retrograde processes linked to rock exhumation (Li *et al.*, 2016). Despite this, Turner *et al.* (2018) recently showed that the unusually light δ^{56}Fe values (down to – 0.31 ‰) of some sub-arc mantle xenoliths were too fractionated to have been caused solely by partial melting. They observed correlations between δ^{56}Fe with $^{206}Pb/^{204}Pb$ and U/Th, tracers of fluid-related processes, and suggested that sample δ^{56}Fe was modified by reaction with low δ^{56}Fe slab fluids. Similar conclusions were reached by Debret *et al.* (2018) who analysed metamorphic gem olivines in veins from the sub-arc mantle of the Kohistan-Ladakh arc. The vein-forming minerals are interpreted to have crystallised from fluids that migrated through the forearc mantle, and they display light δ^{56}Fe (-0.06 to -0.36 ‰) relative to typical mantle olivine (~ +0.01 ‰; Sossi *et al.*, 2015). These results suggest a strong coupling between slab-derived fluids and the δ^{56}Fe composition of the mantle wedge.

To test this idea we carried out a δ^{56}Fe study of serpentinite clasts from the Mariana forearc. The Mariana forearc is the only place in the world where actively metasomatised forearc can be sampled (Savov *et al.*, 2007; Fryer *et al.*, 2018). It belongs to a non-accretionary subduction system, spreading from near Tokyo (Japan) to beyond Guam (U.S.A.) and involves the subduction of the Mesozoic Pacific plate below the Philippine

1. Université de Paris, Institut de physique du globe de Paris, CNRS UMR 7154, 1 rue Jussieu, 75005 Paris, France
2. Department of Earth Sciences, University of Cambridge, Downing Street, Cambridge CB2 3EQ, United Kingdom
3. Laboratoire G-Time, DGES, Université Libre de Bruxelles, ULB, CP 160/02, 1050 Brussels, Belgium
4. School of Earth and Environment, University of Leeds, Leeds, LS2 9JT, United Kingdom
* Corresponding author (email: debret@ipgp.fr)

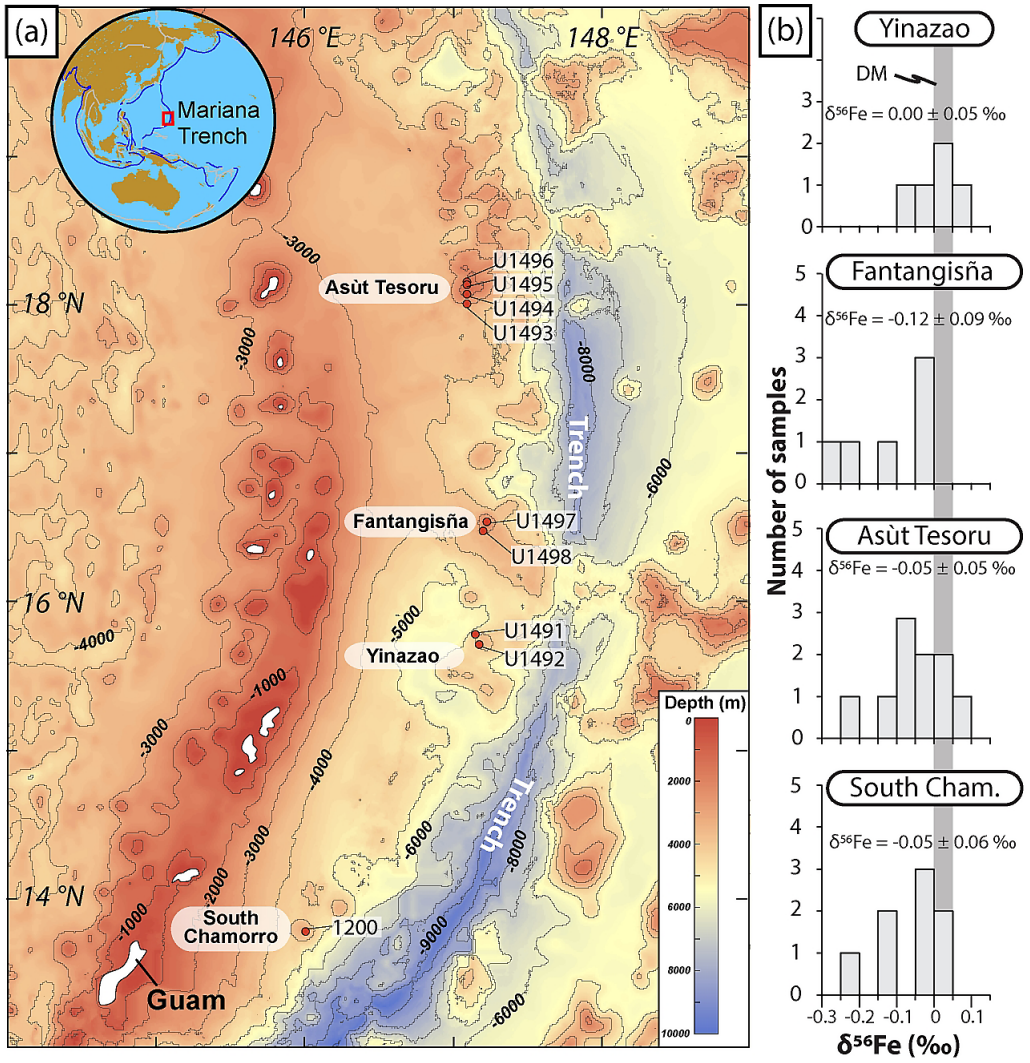

Figure 1 Distribution of δ^{56}Fe values in forearc serpentinites. **(a)** Bathymetry map of the Mariana subduction system showing the locations of the mud volcanoes drilled during IODP Expedition 366 and the ODP Leg 195. Hole locations are indicated in red circles. **(b)** Iron isotope compositions of bulk ultramafic clasts from the Mariana forearc, organized according to the distance from the trench. DM: Depleted Mantle (Craddock *et al.*, 2013).

Sea plate (Fig. 1). Here, fluids released from the subducting slab bring metasomatised forearc rocks to the surface and erupt as mud volcanoes. These rocks provide a direct window into δ^{56}Fe and redox exchanges between the subducted slab and the forearc mantle at various depths. Our study focuses on serpentinised forearc peridotite clasts recovered during the International Oceanic Discovery Program (IODP) Expedition 366 by drilling three mud volcanoes: Yinazao, Fantangisña and Asùt Tesoru, located at increasing distance from the trench (Table S-1, Fig. 1).

Sample Selection

The studied clasts have been petrographically and geochemically characterised by Debret *et al.* (2019) and Fryer *et al.* (2018). They provide a record of deep forearc mantle serpentinisation by slab-derived fluids. Lizardite-bearing serpentinites (Liz-serpentinites) display variable degrees of serpentinisation (from 30 to 100 %) and are primarily composed of low temperature brown serpentine (*i.e.* lizardite and/or chrysotile) and Fe-rich brucite assemblages forming mesh and bastite textures after olivine and orthopyroxene, respectively. These samples represent the first stage of forearc mantle wedge hydration at low temperature (180-230 °C, based on oxygen isotope estimates) and shallow depths (<13 km; Debret *et al.*, 2019). Antigorite-bearing serpentinites (Atg/Liz- and Atg-serpentinites) are highly serpentinised (~ 100 %) and show progressive replacement of lizardite-bearing textures (*i.e.* mesh and bastite) by antigorite, magnetite and Fe-poor brucite. Oxygen isotope measurements show that the recrystallisation of lizardite to antigorite occurs at temperatures ranging from 200-250 °C to 320-410 °C (Debret *et al.*, 2019), consistent with thermodynamic predictions (Evans, 2004) and antigorite crystallisation temperature estimates derived from meta-ophiolite serpentinites (Schwartz *et al.*, 2013). This provides evidence for the formation of these samples during the progressive burial and hydration of the forearc mantle at depths ranging from 13 to 18 km. The recrystallisation of lizardite to antigorite is accompanied by a decrease in Cs, Li and Sr, and an increase in As and Sb concentrations in the bulk clasts, whereas B concentrations are relatively constant (Debret *et al.*, 2019). The forearc wedge also experienced late stage serpentinisation at low temperature (<180 °C) during clast exhumation which is characterised by the crystallisation of "blue" serpentine and sulfides (blue-serpentinite; Debret *et al.*, 2019). Where present, this late serpentinisation stage largely replaces former textures, *i.e.* serpentine or mantle minerals, and results in a flattening of rare earth element (REE) spectra and an increase in bulk serpentinite Zn concentration. In order to constrain the impact of such late retrogression stages on the Fe redox state and isotope composition of forearc peridotites,

we analysed a suite of these blue-serpentinites. Finally, we tested the chemical and Fe-isotope variability of serpentinised clasts along the Mariana forearc by analysing a suite of ultramafic clasts recovered from South Chamorro, one of the most distant mud volcanoes from the trench located at the extreme south of the Mariana subduction, during the Ocean Drilling Program (ODP) Leg 195 (Fig. 1).

Results

The δ^{56}Fe and FeO methods and data (samples and standards) are provided in the Supplementary Information. The Mariana ultramafic clasts display large variations in $Fe^{3+}/\Sigma Fe$ (0.24 – 0.67) and δ^{56}Fe (-0.26 ± 0.06, 2s.d., to +0.09 ± 0.02 ‰; Table S-2) with a light mean δ^{56}Fe of -0.06 ± 0.03 ‰ relative to that of the depleted mantle, as estimated from abyssal peridotites (+0.025 ± 0.025 ‰; Craddock *et al.*, 2013). No systematic variations in $Fe^{3+}/\Sigma Fe$ and δ^{56}Fe values were observed with increasing distance to the trench or mud volcano location (Fig. 1). In contrast, there is a progressive increase in $Fe^{3+}/\Sigma Fe$ and decrease in δ^{56}Fe from Liz- serpentinites ($Fe^{3+}/\Sigma Fe$ = 0.24 – 0.37; δ^{56}Fe = -0.02 ± 0.12 ‰) to Atg/Liz- ($Fe^{3+}/\Sigma Fe$ = 0.33 – 0.59; δ^{56}Fe = -0.07 ± 0.09 ‰) and Atg- ($Fe^{3+}/\Sigma Fe$ = 0.51 – 0.67; δ^{56}Fe = -0.12 ± 0.07 ‰) serpentinites. These variations are broadly correlated with increasing bulk rock fluid-mobile element (FME) concentrations (Fig. 2). In contrast, blue-serpentinites display a large range of $Fe^{3+}/\Sigma Fe$ (0.33 – 0.77) with depleted mantle-like δ^{56}Fe (-0.01 ± 0.03 ‰) and correlations with FME concentrations are absent (Table S-2, Fig. S-1a-c).

Discussion

The low δ^{56}Fe signatures of antigorite-bearing clasts agree with our prediction that isotopically light Fe is mobilised in slab fluids (*e.g.*, Debret *et al.*, 2016, 2018). However, before assigning all Fe isotope variability to fluids, several processes must be considered: (1) pre-existing Fe isotope mantle heterogeneities prior to the forearc serpentinisation and (2) the mobility of Fe during late serpentinisation stages accompanying clast exhumation (*e.g.*, blue-serpentine crystallisation). The influence of kinetic effects, related to the preferential mobility of isotopically light species during fluid/rock interactions or diffusive processes, can be ruled out as the direction of diffusive transport from solid (Fe-rich) to fluid (Fe-poor) would result in enrichment in isotopically heavy Fe in the solid, which would generate positive covariations between δ^{56}Fe and $Fe^{3+}/\Sigma Fe$ in the studied samples, which are not observed (Fig. 2c).

Forearc mantle wedge peridotites are former sub-arc peridotites that underwent extensive partial melting before being dragged into the forearc by mantle convection (Parkinson and Pearce, 1998). In serpentinised peridotites, protolith fertility is better assessed by Al_2O_3/SiO_2 ratio rather than Al_2O_3 contents (Niu, 2004). The Mariana ultramafic clasts display low Al_2O_3/SiO_2 (<0.03) consistent with a refractory protolith, *i.e.* dunite or pyroxene-poor harzburgite. However, the studied samples also display a large range in δ^{56}Fe relative to dunite-like reference materials (Table S-2) and no systematic variation between δ^{56}Fe and Al_2O_3/SiO_2 ratio are observed (Fig. S-2a). Similarly, previous studies have shown that high temperature metasomatic events (*e.g.*, melt percolation) can lead to an enrichment in isotopically light Fe (Poitrasson *et al.*, 2013). However, such processes also generate an increase in FeO and correlation between δ^{56}Fe and XMg (= Mg / [Mg + Fe]) are not observed in the studied samples (Fig. S-2b). This

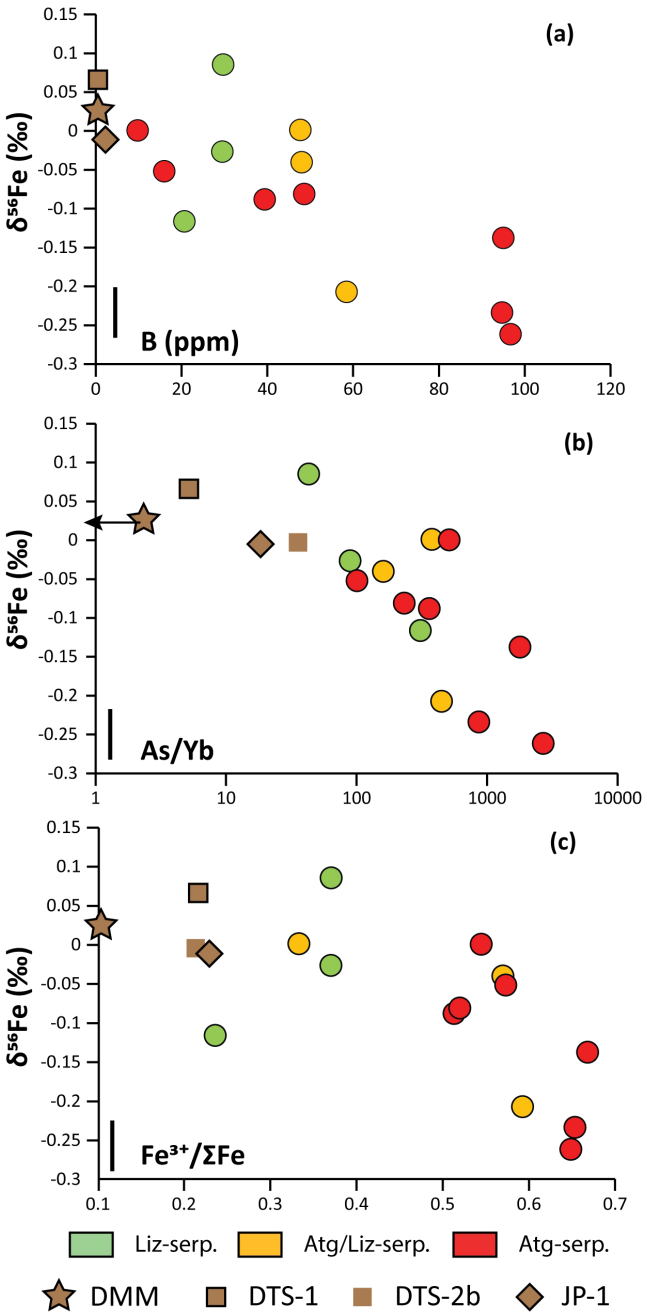

Figure 2 Plots of δ^{56}Fe *versus* **(a)** B concentrations, **(b)** As/Yb and **(c)** $Fe^{3+}/\Sigma Fe$ ratios in Mariana ultramafic clasts. The black bar represents the FeCl standard reproducibility during analyses. DTS-1, DTS-2b, JP-1: dunite-like reference materials.

shows that the light δ^{56}Fe of Mariana clasts are not controlled by pre-existing protolith heterogeneities and must have been generated by the mobilisation of Fe in fluids.

Late serpentinisation stages that overprint high temperature paragenesis are associated with exhumation of clasts and are characterised by blue-serpentine crystallisation and changes in trace element chemistry (Debret *et al.*, 2019). However, despite strong enrichments in Zn, blue-serpentinites display similar δ^{56}Fe (from -0.07 ‰ to +0.05 ‰) to depleted mantle, dunite reference materials and abyssal peridotites (Fig. S-3). Similarly, no correlation between δ^{56}Fe and indices of late processes, for example, seafloor carbonation (*e.g.*, Sr/Yb) and/or blue-serpentine (*e.g.*, Zn) crystallisation, are observed (Fig. S-3). This suggests that the Mariana forearc clasts preserved δ^{56}Fe values acquired prior to exhumation.

The light $\delta^{56}Fe$ of our samples must therefore relate either to the loss or the addition of Fe during the serpentinisation of the forearc mantle at depth.

It is well established that forearc mantle serpentinisation by slab-derived fluids is accompanied with an increase in bulk rock FME concentrations (*e.g.*, Savov *et al.*, 2007). This enrichment has been attributed to the influx of slab-derived fluids in the forearc mantle at intermediate temperatures (200-600 °C). In Figure 2a,b, the prograde Mariana ultramafic clasts (Liz-, Atg/Liz- and Atg-serpentinites) form a step array that extends from mantle-like to low $\delta^{56}Fe$ values (-0.26 ‰); this is accompanied with an increase in FME concentrations. In contrast, no correlation between $\delta^{56}Fe$ and FME concentrations is observed in retrograde blue-serpentinites or abyssal serpentinites (Fig. S-1a,b). The light $\delta^{56}Fe$ of the studied samples therefore must reflect the addition of isotopically light Fe by slab-derived fluids. Furthermore, this decrease in $\delta^{56}Fe$ is associated with an increase in $Fe^{3+}/\Sigma Fe$ (Fig. 2c), which is opposed to isotope theory predicting that isotopically heavy Fe will be concentrated into Fe^{3+}-bearing phases rather than Fe^{2+}-bearing phases (Polyakov and Mineev, 2000). This observation thus rules out the direct transfer of Fe^{3+} by slab-derived fluids. Instead, it suggests a concomitant transfer of isotopically light Fe^{2+} complexed with an oxidising component (*e.g.*, sulfate or carbonate) in slab-derived fluids. Both sulfate or carbonate complexes have the potential to modify both the Fe isotope signature and oxidation state of forearc serpentinites, despite the relatively low solubility of Fe in fluids (Debret *et al.*, 2018). Although chlorine complexes (*e.g.*, $Fe(II)Cl_2$), also preferentially complex light Fe, they are inefficient oxidisers of Fe, and thus an unlikely means of generating the observed relationships between $\delta^{56}Fe$ and $Fe^{3+}/\Sigma Fe$ (Fig. 2c).

Differences in the stability fields of hydrous, carbon- and sulfur-bearing minerals mean that the compositions of fluid liberated from the subducting slab change progressively with depth. Because of the pronounced differences in $\delta^{56}Fe$ between the Liz- and Atg-serpentinite clasts, it is important to identify the reactions responsible for the transfer of isotopically light and oxidised Fe to the mantle wedge. The serpentinisation of mantle peridotites through their interaction with water is commonly associated with the oxidation of ferrous Fe, leading to a progressive increase of $Fe^{3+}/\Sigma Fe$ in the bulk rock and H_2 production in the fluid phase through water reduction (Fig. 3):

$$3\ FeO + H_2O_{(aq)} = Fe_3O_4 + H_{2(aq)} \qquad \text{Eq. 1}$$

This process is expected to be efficient at the relatively low temperature of forearc serpentinisation (*i.e.* lower than 700 °C; Frost and Ballhaus, 1998). It can explain why the Mariana ultramafic clasts have high $Fe^{3+}/\Sigma Fe$ ratios (0.24 – 0.67) relative to mantle peridotites (~ 0.1; Canil *et al.*, 1994). However, no obvious correlations between bulk rock water content and Fe redox state or between bulk rock water content and $\delta^{56}Fe$ are observed (Fig. S-4). Light $\delta^{56}Fe$ are mainly observed in antigorite-bearing samples while lizardite-bearing serpentinite displays depleted mantle-like values (Fig. 2). This suggests a marked change in the composition of slab-derived fluids with depth, where the composition of fluids derived at greater depths preferentially mobilise Fe relative to fluids released at shallower levels. Fluids released during the early (shallow) stage of slab devolatilisation (<13 km depth) are likely dominated by diagenetic processes and opal dehydration, whereas later (deeper) processes can include decarbonation and clay mineral decomposition reactions (Bebout, 2013 and references therein). Arsenic, Sb and light REE are preferentially enriched in fluids derived from sediment or metabasite decarbonation reactions (Bebout, 2013). The correlation between As/Yb and $\delta^{56}Fe$ in ultramafic clasts (Fig. 2b) may therefore indicate light $\delta^{56}Fe$ is transferred to the mantle wedge by carbonate complexes. The transfer of redox sensitive elements, such as carbon, can modify the redox state of the forearc mantle according to the reaction (Fig. 3):

$$2FeCO_{3(aq)} + 6FeO = 4Fe_2O_3 + 2C \qquad \text{Eq. 2}$$

The exact form of carbon in this equation is speculative. However, the increase of $Fe^{3+}/\Sigma Fe$ in the ultramafic clasts is consistent with the observed increase of complex abiotic hydrocarbon phases in pore fluids from the most distal mud

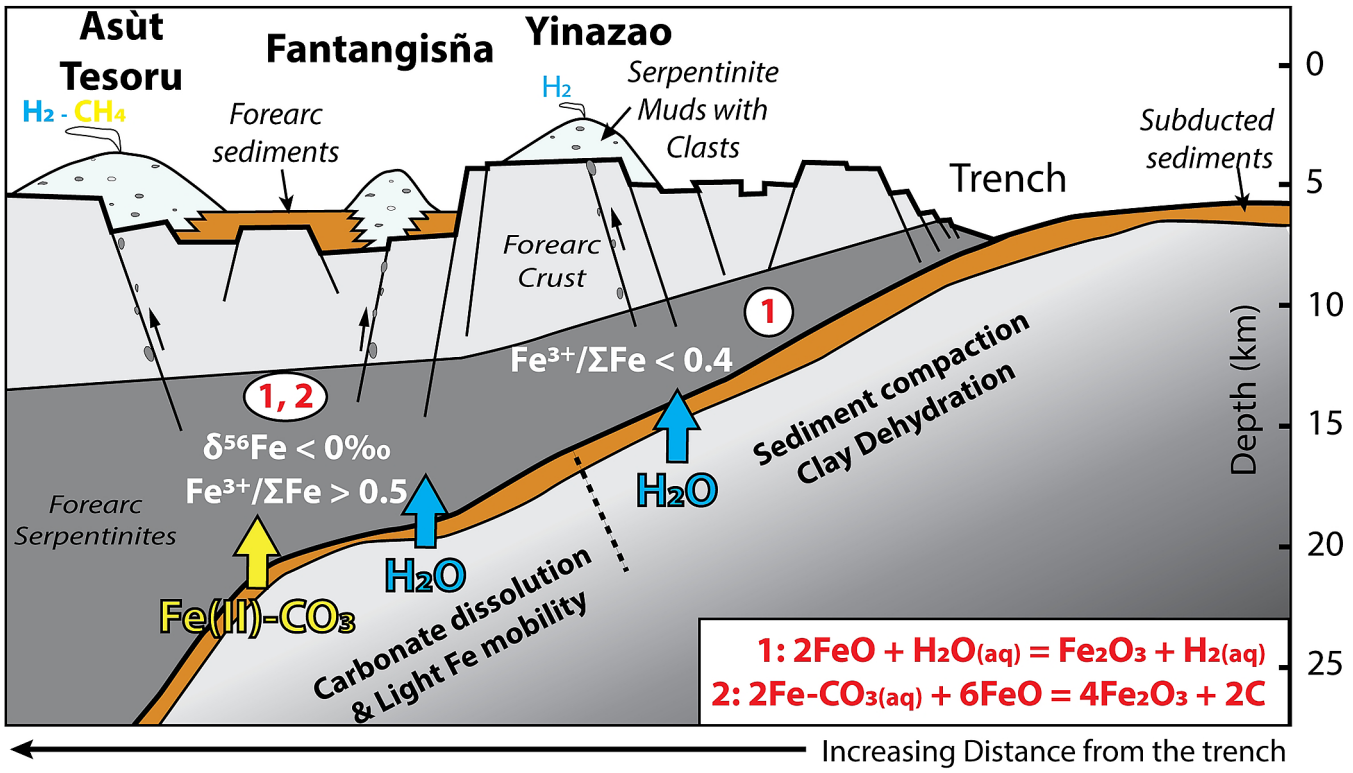

Figure 3 Cartoon illustrating redox and isotopic transfers between the slab and the forearc mantle wedge.

volcanoes (Eickenbusch *et al.*, 2019), suggesting that carbon may be the relevant oxidising agent in this setting. Furthermore, several studies have speculated the sulfate anions, derived from hydrous breakdown of sulfides, can complex with Fe and facilitate its transfer to the mantle wedge, for example:

$$FeSO_{4(aq)} + 12FeO = 4Fe_3O_4 + FeS \qquad \text{Eq. 3}$$

Reactions of this type are consistent with several studies which have shown that progressive prograde metamorphism of the subducting slab is associated with the release of sulfate- and/or carbonate-bearing fluids that mobilise light $\delta^{56}Fe$ (Debret *et al.*, 2016, 2018). The percolation of such fluids into the forearc can drive Fe oxidation and therefore explain the negative correlation between $\delta^{56}Fe$ and $Fe^{3+}/\Sigma Fe$ (Fig. 2c), despite the absence of a correlation with bulk rock water contents (Fig. S-4).

The oxygen fugacity (fO_2) of slab-derived fluids is believed to increase with depth (*e.g.*, Debret *et al.*, 2016), with high fO_2 conditions (*e.g.*, magnetite/hematite buffer) occurring at eclogite facies conditions (~ 80 km depth). Thus, during shallow forearc hydration (13-18 km depth), sulfur is expected to be equilibrated at modest fO_2 in slab-derived fluids and mainly transferred under reduced form (*e.g.*, H_2S), while carbon will be equilibrated as an oxidised form (CO_2). It is thus plausible to consider that carbonate could be the main ligand transferring isotopically light Fe from the slab to the shallow mantle wedge. This is consistent with the high carbon concentrations measured in Mariana pore fluids from the most distant mud volcanoes (Fryer *et al.*, 2018). Together, the correlation between Fe isotopes, FME concentrations and ratios, and iron redox state demonstrate a critical role for slab-derived fluids in regulating the redox state of the mantle wedge.

Acknowledgements

This research used samples and data provided by the IODP and ODP. We are grateful to the crew of the D/V JOIDES Resolution and to the science party of IODP Expedition 366. Funding for this research was provided by a NERC Moratorium Award (NE/P020860/1, to BD and HMW), the F.R.S.-F.N.R.S. (BD), the Fondation Wiener Anspach (RG97553, NM, BD and HMW), the ERC Consolidator Grant (306655, HMW), a NERC Critical Minerals grant (NE/M010848/1, HMW) and a Schlanger Fellowship Award (IS). We thank K. Evans and F. Poitrasson for critical comments on earlier version of this article and careful editorial handling by M. Boyet. This study contributes to the IdEx Université de Paris ANR-18-IDEX-0001.

Editor: Maud Boyet

Additional Information

Supplementary Information accompanies this letter at http://www.geochemicalperspectivesletters.org/article2003.

Cite this letter as: Debret, B., Reekie, C.D.J., Mattielli, N., Beunon, H., Ménez, B., Savov, I.P., Williams, H.M. (2020) Redox transfer at subduction zones: insights from Fe isotopes in the Mariana forearc. *Geochem. Persp. Let.* 12, 46–51.

References

Bebout, G.E. (2013) Chemical and Isotopic Cycling in Subduction Zones. *Treatise on Geochemistry: Second Edition* 4, 703–747, doi: 10.1016/B978-0-08-095975-7.00322-3.

Canil, D., O'Neill, H.S.C., Pearson, D.G., Rudnick, R.L., McDonough, W.F., Carswell, D.A. (1994) Ferric iron in peridotites and mantle oxidation states. *Earth and Planetary Science Letters* 123, 205–220.

Craddock, P.R., Warren, J.M., Dauphas, N. (2013) Abyssal peridotites reveal the near-chondritic Fe isotopic composition of the Earth. *Earth and Planetary Science Letters* 365, 63–76.

Debret, B., Millet, M.-A., Pons, M.-L., Bouilhol, P., Inglis, E., Williams, H. (2016) Isotopic evidence for iron mobility during subduction. *Geology* 44, 215–218.

Debret, B., Bouilhol, P., Pons, M.L., Williams, H. (2018) Carbonate Transfer during the Onset of Slab Devolatilization: New Insights from Fe and Zn Stable Isotopes. *Journal of Petrology* 59, 1145–1166.

Debret, B. *et al.* (2019) Shallow forearc mantle dynamics and geochemistry: New insights from the IODP expedition 366. *Lithos* 326–327, 230–245.

Eickenbusch, P., Takai, K., Sissman, O., Suzuki, S., Menzies, C. (2019) Origin of Short-Chain Organic Acids in Serpentinite Mud Volcanoes of the Mariana Convergent Margin. *Frontiers in Microbiology* 10, 1–21.

Evans, B.W. (2004) The Serpentinite Multisystem Revisited: Chrysotile Is Metastable. *International Geology Review* 46, 479–506.

Evans, K.A. (2012) The redox budget of subduction zones. *Earth-Science Reviews* 113, 11–32.

Frost, B.R., Ballhaus, C. (1998) Comment on "Constraints on the origin of the oxidation state of mantle overlying subduction zones : An example from Simcoe , Washington , USA". *Geochimica et Cosmochimica Acta* 62, 329–331.

Fryer, P., Wheat, C.G., Williams, T., Scientists Expedition, 366 (2018) Mariana Convergent Margin and South Chamorro Seamount. *Proceedings of the International Ocean Discovery Program* 366.

Huang, J., Guo, S., Jin, Q.-Z., Huang, F. (2019) Iron and magnesium isotopic compositions of subduction-zone fluids and implications for arc volcanism. *Geochimica et Cosmochimica Acta,* doi: 10.1016/j.gca.2019.06.020.

Kelley, K.A., Cottrell, E. (2009) Water and the oxidation state of subduction zone magmas. *Science* 325, 605–607.

Li, D.Y., Xiao, Y.L., Li, W.Y., Zhu, X., Williams, H.M., Li, Y.L. (2016) Iron isotopic systematics of UHP eclogites respond to oxidizing fluid during exhumation. *Journal of Metamorphic Geology* 34, 987–997.

Nebel, O., Sossi, P.A., Bénard, A., Wille, M., Vroon, P.Z., Arculus, R.J. (2015) Redox-variability and controls in subduction zones from an iron-isotope perspective. *Earth and Planetary Science Letters* 432, 142–151.

Niu, Y. (2004) Bulk-rock major and trace element compositions of abyssal peridotites: Implications for mantle melting, melt extraction and post-melting processes beneath Mid-Ocean ridges. *Journal of Petrology* 45, 2423–2458.

Parkinson, I.J., Pearce, J.A. (1998) Peridotites from the Izu-Bonin-Mariana forearc (ODP Leg 125): evidence for mantle melting and melt-mantle interaction in a supra-subduction zone setting. *Journal of Petrology* 39, 1577–1618.

Poitrasson, F., Delpech, G., Gregoire, M. (2013) On the iron isotope heterogeneity of lithospheric mantle xenoliths : implications for mantle metasomatism , the origin of basalts and the iron isotope composition of the Earth. *Contributions to Mineralogy and Petrology* 165, 1243–1258.

Polyakov, V.B., Mineev, S.D. (2000) The use of Mossbauer spectroscopy in stable isotope geochemistry. *Geochimica et Cosmochimica Acta* 64, 849–865.

Savov, I.P., Ryan, J.G., D'Antonio, M., Fryer, P. (2007) Shallow slab fluid release across and along the Mariana arc-basin system: Insights from geochemistry of serpentinized peridotites from the Mariana fore arc. *Journal of Geophysical Research: Solid Earth* 112, B09205.

Schwartz, S., Guillot, S., Reynard, B., Lafay, R., Debret, B., Nicollet, C., Lanari, P., Auzende, A.L. (2013) Pressure-temperature estimates of the lizardite/antigorite transition in high pressure serpentinites. *Lithos* 178, 197–210.

Sossi, P.A., Halverson, G.P., Nebel, O., Eggins, S.M. (2015) Combined separation of Cu, Fe and Zn from rock matrices and improved analytical protocols for stable isotope determination. *Geostandards and Geoanalytical Research* 39, 129–149.

Turner, S., Williams, H., Piazolo, S., Blichert-Toft, J., Gerdes, M., Adam, J., Liu, X.M., Schaefer, B., Maury, R. (2018) Sub-arc xenolith Fe-Li-Pb isotopes and textures tell tales of their journey through the mantle wedge and crust. *Geology* 46, 947–950.

Williams, H.M., McCammon, C.A., Peslier, A.H., Halliday, A.N., Teutsch, N., Levasseur, S., Burg, J.P. (2004) Iron isotope fractionation and the oxygen fugacity of the mantle. *Science* 304, 1656–1659.

Geochemical Perspectives Letters

Redox transfer at subduction zones: insights from Fe isotopes in the Mariana forearc

B. Debret, C.D.J. Reekie, N. Mattielli, H. Beunon, B. Ménez, I.P. Savov, H.M. Williams

Supplementary Information

The Supplementary Information includes:

- Method
- Tables S-1 and S-2
- Figures S-1 to S-4
- Supplementary Information References

Method

Major and trace elements compositions of the ultramafic clasts are from Debret *et al.*, 2019. FeO analyses of bulk-rock (BR) samples were performed at the SARM-CRPG (Nancy, France). These analyses were done by automatic titration at the equivalent point with potassium dichromate after dissolution of the sample in a HF/H_2SO_4 mixture, in the presence of H_3BO_3 and H_3PO_4. Subsequently, $Fe^{3+}/\Sigma Fe$ ratios were calculated from the measured $Fe_2O_3^{Tot}$ (BR) and FeO^{Tot} (BR) values. The error on the FeO analyses is lower than 0.05 wt. % (2sd) based on repeated analyses of UB-N serpentinite standard (CRPG-standard). The method has been tested by Debret *et al.* (2015), who were able to match measured bulk $Fe^{3+}/\Sigma Fe$ ratios with those recalculated from µ-XANES measurements of serpentine minerals (see Debret *et al.*, 2014, 2015 for method details, including standards, precision and calibration data for XANES measurements). Reference material values UB-N (FeO = 2.86 wt. %) and BIR (FeO = 8.59 wt. %) are in agreement with previous studies (e.g., Amonette and Scott, 1991; $FeO_{(UB\text{-}N)}$ = 3.01 wt. %; $FeO_{(BIR)}$ = 8.53 wt. %).

For Fe isotope measurements, ~50 mg of powdered samples were dissolved using a 1:1 mix of concentrated HF and HCl in Parr bombs at 160 °C in an oven for 5 days. These were then further dissolved with aqua regia, a 1:3 mix of concentrated HNO_3 and HCl, for 3 days at 130 °C. Finally, samples were brought into solution in 6 M HCl prior to column chemistry. This intensive procedure ensures full dissolution of refractory phases such as spinel. Quantitative purifications of Fe were achieved by chromatographic exchange, using 1 ml of AG1-x8 (200–400 mesh) and 0.4 × 7 cm Teflon columns, following the procedure developed by Sossi *et al.* (2015). All reagents used in the chemistry and mass spectrometry procedures were distilled and subboiled using Teflon two-bottle stills. The total procedural blank contribution was < 80 ng of Fe, which is negligible compared to the amount of Fe loaded on the columns (blank contribution is << 1%). Iron isotopes analyses were obtained at the University of Cambridge (UK) on a Thermo Neptune Plus multiple-collector inductively coupled plasma mass spectrometer (MC-ICP-MS). The analyses were performed in wet plasma mode. Instrumental mass fractionation was corrected by sample-standard bracketing to the IRMM-014 Fe standard.

During MC-ICP-MS measurements, analysed solutions consisted of 2 ppm natural Fe in 0.1M HNO3. The Fe beam intensities in medium resolution mode typically varied between 25 and 35V ^{56}Fe for a standard $10^{11}\Omega$ resistor. Isotope ratios are reported as $\delta^{56}Fe$ in permil notation relative to IRMM-014 external standard, and $\delta^{57}Fe$ is given to demonstrate mass dependency of the measurements. All reported errors are 2 standard deviations (2sd).

$$\delta^{56}Fe = ((^{56}Fe/^{54}Fe_{sample}) / (^{56}Fe/^{54}Fe_{IRMM\text{-}014}) - 1) \times 10^3$$

$$\delta^{57}Fe = ((^{57}Fe/^{54}Fe_{sample}) / (^{57}Fe/^{54}Fe_{IRMM\text{-}014}) - 1) \times 10^3$$

Mass dependence, long-term reproducibility and accuracy were evaluated by repeated analysis of an in-house FeCl salt standard ($\delta^{56}Fe$ = -0.73 ± 0.03 ‰; $\delta^{57}Fe$ = -1.08 ± 0.06 ‰ 2sd, n = 50) previously analysed in other studies (Millet *et al.*, 2012; Weyer and Ionov, 2007; Williams and Bizimis, 2014). In addition, reference materials (UB-N serpentinites, JP-1, DTS-2b and PCC1 peridotites) were processed through columns and analysed for Fe stable isotopes alongside samples. The data for these are displayed in Table S-1 and are in good agreement with previous studies.

Supplementary Tables

Table S-1 Critical parameters of the Mariana mud volcanoes (after Fryer *et al.*, 2018). Depth-to-slab was determined by seismic reflection profile for Yinazao, Fantangisña and Asùt Tesoro (Oakley *et al.*, 2007, 2008; Oakley, 2008), and by equilibrium mineral assemblages in metamafic clasts for South Chamorro (Maekawa *et al.*, 1993; Fryer *et al.*, 2006). Distance to trench and temperature of slab from Hulme *et al.* (2010). Depth-to-slab measurements for Yinazao, Fantangisna, and Asùt Tesoro from Oakley *et al.* (2008) and Oakley (2008). Depth-to-slab measurements for South Chamorro are extrapolation estimates (see Fryer *et al.*, 2018).

	Yinazao	Fantangisña	Asùt Tesoru	S. Chamorro
Distance to trench (km)	55	62	72	78
Depth to slab (km)	13	14	18	19
Temperature of slab (°C)	~80°	~150°	~250°	~300°

Table S-2 Iron redox state ($Fe^{3+}/\Sigma Fe$) and isotope analyses ($\delta^{56}Fe$ and $\delta^{57}Fe$, in ‰) of the studied samples. The trace element data are from Debret *et al.* (2019), B and Zn concentrations are reported in ppm.

Seamount	Label identifier	$Fe^{3+}/\Sigma Fe$	$\delta^{56}Fe$	2sd	$\delta^{57}Fe$	2sd	n	Al_2O_3/SiO_2	B	Zn	As/Yb	Sr/Yb
IODP expedition 366												
Blue Serpentinites:												
Yinazao	U1492C-5F-2-W 25/28	0.33	0.05	0.03	0.08	0.03	6	0.007	7	73		
Yinazao	U1492C-5F-3-W 43/47	0.66	-0.07	0.05	-0.10	0.09	3	0.022	6.7	73	40	914
Yinazao	U1492A-1H-2-W 139/140	0.77	0.00	0.02	0.03	0.13	3	0.020	240	66	45	212
Yinazao	U1492A-1H-3-(115-135)	0.69	0.05	0.01	0.08	0.04	3	0.024	165	61	30	281
Yinazao	U1492C-12F-2-W 19/22	0.56	-0.01	0.02	-0.01	0.02	6	0.020	7.9	58	37	986
Fantangisña	U1497A-3G-CC-W 9/10	0.62	-0.01	0.05	-0.03	0.03	3	0.015	93	76	139	262
Fantangisña	U1498B-3R-3-W 89/92	0.58	-	-	-	-	-	0.016	18.7	100	83	611
Fantangisña	U1498B-13R-1-W 37/45	0.46	-0.04	0.02	-0.05	0.03	6	0.024	26.7	56	97	500
Asùt Tesoru	U1496B-5F-1-W 77/82	0.56	-0.02	0.04	-0.05	0.07	3	0.017	10.7	96	84	778
Liz-Serpentinites:												
Asùt Tesoru	U1493B-9X-1-W 56/58	0.24	-0.12	0.03	-0.17	0.03	4	0.008	20.7	48	309	248
Asùt Tesoru	U1493B-9X-CC-W 4/9	0.37	0.09	0.02	0.13	0.03	3	0.020	29.7	65	43	556
Asùt Tesoru	U1493B-9X-CC-W 14/16	0.37	-0.03	0.03	-0.05	0.04	6	0.013	29.5	56	89	775
Atg/Liz-Serpentinites:												
Asùt Tesoru	U1495B-3G-CC-W 5/7	0.59	-0.21	0.05	-0.31	0.03	6	0.011	58.5	49	447	344
Asùt Tesoru	U1495B-3G-CC-W 24/26	0.33	0.00	0.02	0.01	0.04	6	0.003	47.7	48	377	725
Fantangisña	U1497A-13G-CC-W 52/55	0.57	-0.04	0.02	-0.06	0.03	6	0.013	48	55	160	149
Atg-Serpentinites:												
Asùt Tesoru	U1495B-5G-CC-W 17/20	0.57	-0.05	0.05	-0.07	0.05	6	0.016	16	52	101	67
Asùt Tesoru	U1495B-6F-CC-W 10/12	0.54	0.00	0.03	0.01	0.03	6	0.014	9.8	36	512	121
Asùt Tesoru	U1495A-3G-CC-W 13/15	0.51	-0.09	0.01	-0.14	0.02	6	0.021	39.4	44	360	12
Asùt Tesoru	U1495A-4F-1-W 86/89	0.52	-0.08	0.02	-0.12	0.04	6	0.023	48.6	52	232	8
Fantangisña	U1497B-4G-1-W 3/5	0.67	-0.14	0.00	-0.20	0.01	3	0.003	95	33	1783	185
Fantangisña	U1497B-4G-1-W 8/12	0.65	-0.23	0.01	-0.35	0.01	3	0.003	94.7	32	865	85
Fantangisña	U1497B-4G-1-W 3/6	0.65	-0.26	0.06	-0.47	0.07	3	0.003	96.7	33	2696	277

ODP Leg 195 expedition												
South Chamorro	1200A-7R-02-3/5	-	-0.12	0.06	-0.19	0.05	3	-	-	-	-	-
South Chamorro	1200A-11R-01-69/72	-	0.00	0.01	0.01	0.04	3	-	-	-	-	-
South Chamorro	1200A-12R-01-3/5	-	-0.20	0.01	-0.27	0.04	3	-	-	-	-	-
South Chamorro	1200A-15R-01-11/13	-	-0.11	0.03	-0.16	0.07	3	-	-	-	-	-
South Chamorro	1200A-3R-01-81/84	-	0.01	0.01	0.02	0.04	3	-	-	-	-	-
South Chamorro	1200A-13R-02-12/15	-	0.00	0.01	0.01	0.02	3	-	-	-	-	-
South Chamorro	1200A-7R-01-4/6	-	0.01	0.03	0.01	0.06	3	-	-	-	-	-
South Chamorro	1200A-16R-02-48/50	-	-0.02	0.00	0.00	0.00	3	-	-	-	-	-
Standards												
	PCC-1 (peridotite)	-	0.01	0.02	0.02	0.04	4	-	-	-	-	-
	replicate	-	0.01	0.04	0.03	0.05	3	-	-	-	-	-
	JP-1 (dunite)	-	-0.01	0.03	0.01	0.06	3	-	-	-	-	-
	replicate	-	-0.01	0.02	0.00	0.03	3	-	-	-	-	-
	DTS-2b (dunite)	-	0.00	0.02	0.00	0.05	3	-	-	-	-	-
	UB-N (serpentinite)	-	0.04	0.02	0.07	0.03	3	-	-	-	-	-
	replicate	-	0.03	0.01	0.06	0.03	3	-	-	-	-	-

Supplementary Figures

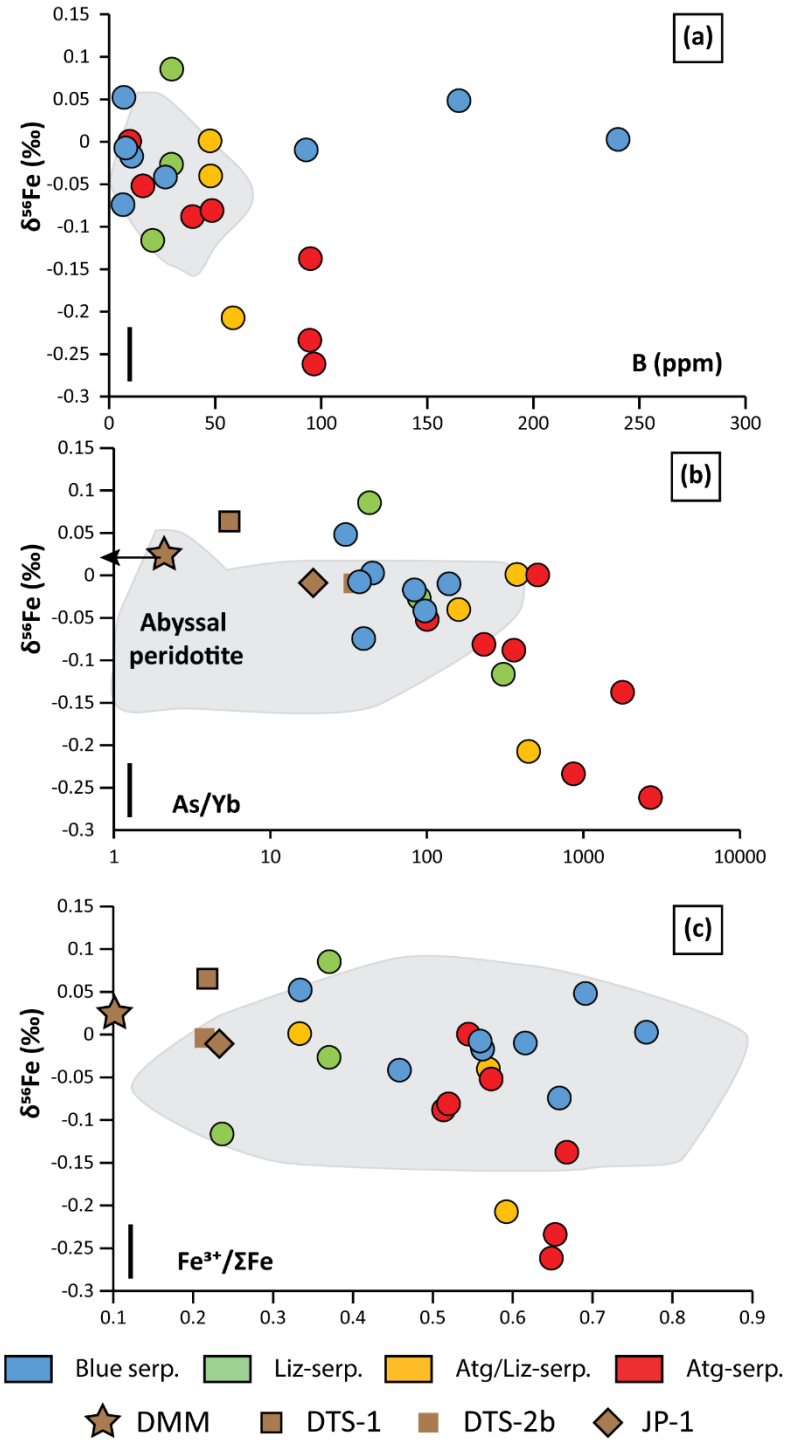

Figure S-1 Plots of $\delta^{56}Fe$ versus slab derived fluids proxies (**a-b**) and $Fe^{3+}/\Sigma Fe$ (**c**). Note that no correlation between blue-serpentinites and slab derived fluids or redox proxies have been observed showing that low pressure serpentinization stages are unable to fractionate Fe isotopes. This is in good agreement with abyssal peridotites analyses which are close to primitive mantle values. The abyssal peridotite field is from Debret *et al.* (2018). The black bars represent the standard reproducibility.

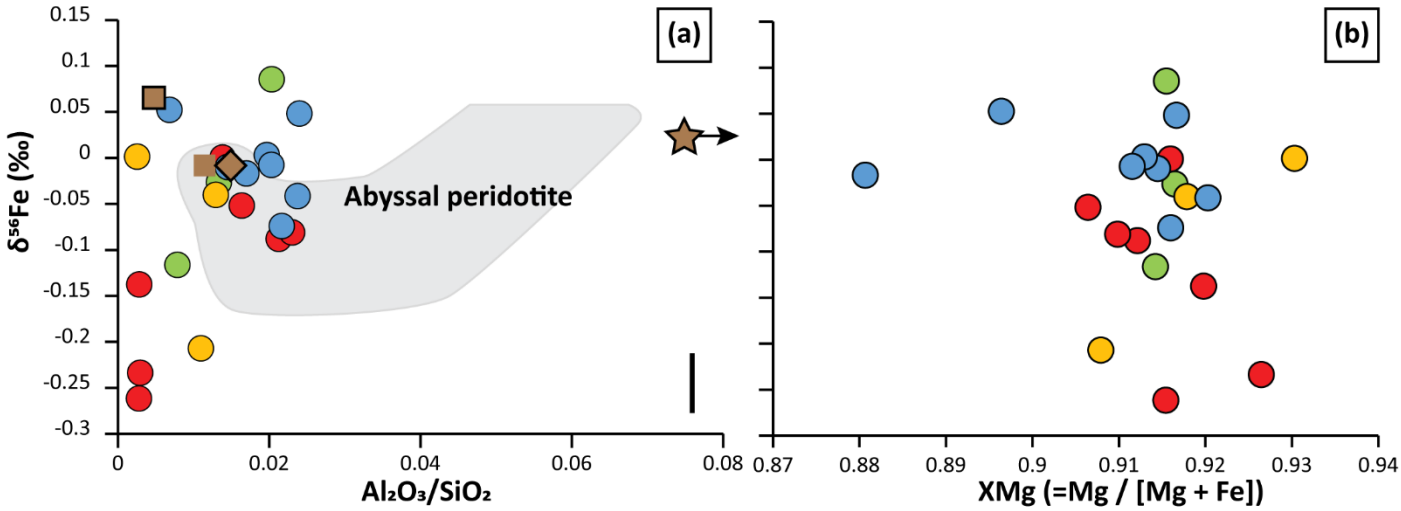

Figure S-2 Plots of δ^{56}Fe versus rock fertility (**a**) and high temperature metasomatic (**b**) proxies. No correlation between δ^{56}Fe and neither rock fertility and high temperature metasomatic proxies have been observed.

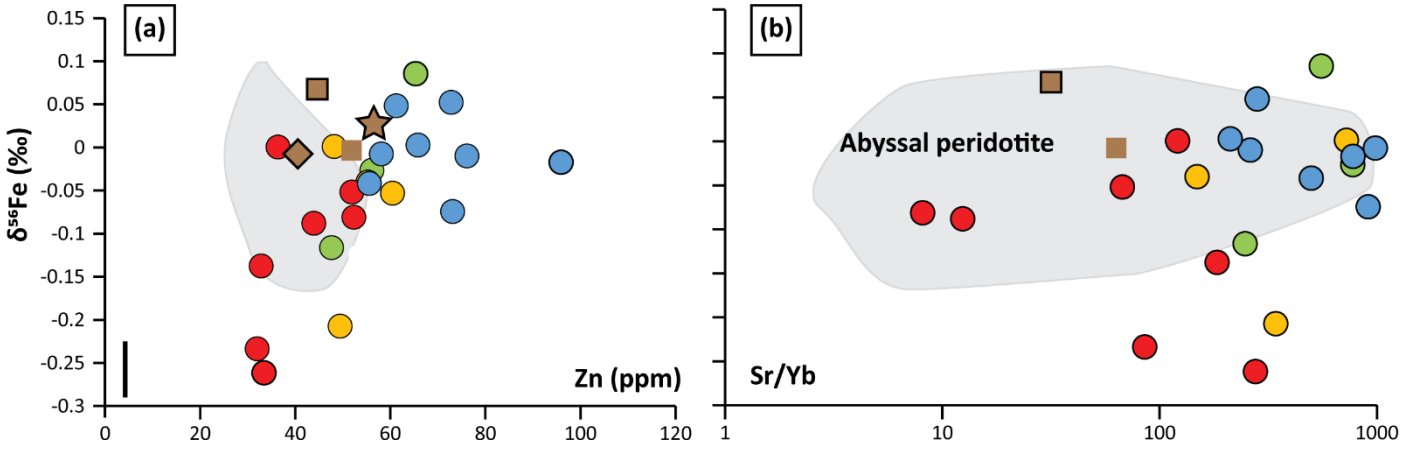

Figure S-3 Plots of δ^{56}Fe versus late stages of serpentinization (**a**) or carbonation (**b**) proxies.

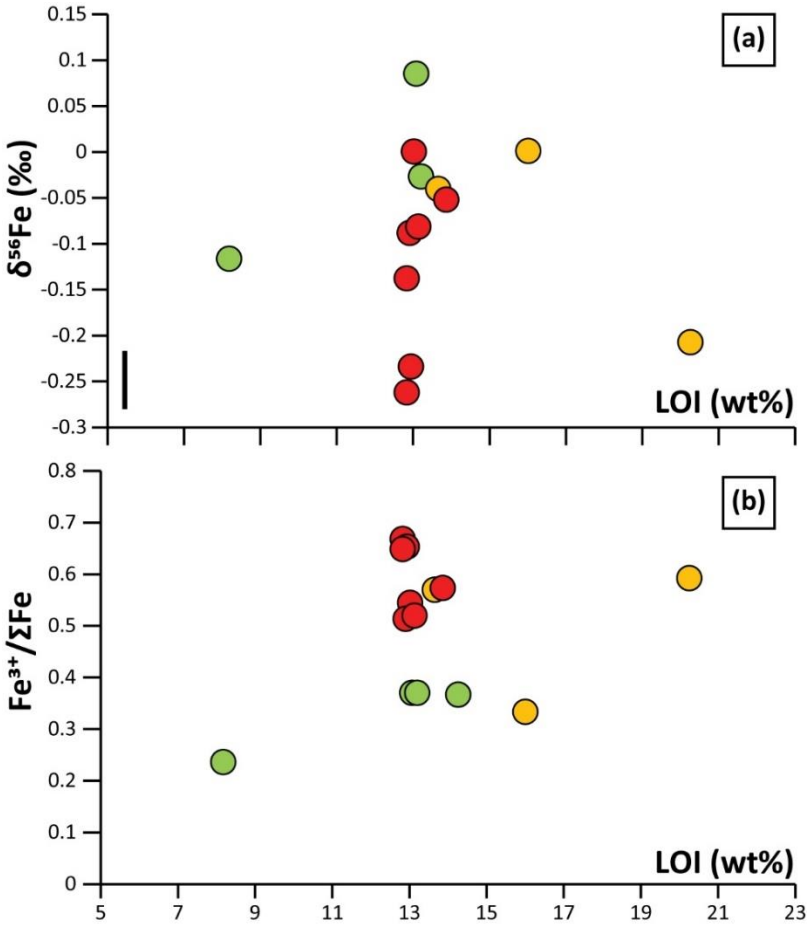

Figure S-4 Plots of δ^{56}Fe (**a**) and $Fe^{3+}/\Sigma Fe$ (**b**) versus serpentinization degree proxy (Loss On Ignition, LOI).

Supplementary Information References

Debret, B., Andreani, M., Muñoz, M., Bolfan-Casanova, N., Carlut, J., Nicollet, C., Schwartz, S., Trcera, N. (2014) Evolution of Fe redox state in serpentine during subduction. *Earth and Planetary Science Letters* 400.

Debret, B., Bolfan-Casanova, N., Padron-Navarta, J.A., Martin-Hernandez, F., Andreani, M., Garrido, C., López Sánchez-Vizcaíno, V., Gómez-Pugnaire, M.T., Muñoz, M., Trcera, N. (2015) Redox state of iron during high-pressure serpentinite dehydration. *Contributions to Mineralogy and Petrology* 169.

Debret, B., Beunon, H., Mattielli, N., Andreani, M., Ribeiro da Costa, I., Escartin, J. (2018a) Ore component mobility, transport and mineralization at mid-oceanic ridges: A stable isotopes (Zn, Cu and Fe) study of the Rainbow massif (Mid-Atlantic Ridge 36°14′N). *Earth and Planetary Science Letters* 503, 170-180.

Debret, B., Bouilhol, P., Pons, M.L., Williams, H. (2018b) Carbonate Transfer during the Onset of Slab Devolatilization: New Insights from Fe and Zn Stable Isotopes. *Journal of Petrology* 59, 1145–1166.

Debret, B., Albers, E., Walter, B., Price, R., Barnes, J. D., Beunon, H., Facq, S., Gillikin, D.P., Mattielli, N., Williams, H., (2019) Shallow forearc mantle dynamics and geochemistry: New insights from the IODP expedition 366. *Lithos* 326–327, 230–245.

Fryer, P., Gharib, J., Ross, K., Savov, I., Mottl, M.J. (2006) Variability in serpentinite mudflow mechanisms and sources: ODP drilling results on Mariana forearc seamounts. *Geochemistry, Geophysics, Geosystems* 7, Q08014.

Fryer, P., Wheat, C.G., Williams, T., Scientists Expedition, 366 (2018) Mariana Convergent Margin and South Chamorro Seamount. *Proceedings of the International Ocean Discovery Program* 366.

Maekawa, H., Shozui, M., Ishii, T., Fryer, P., Pearce, J.A. (1993) Blueschist metamorphism in an active subduction zone. *Nature* 364, 520–523.

Millet, M.A., Baker, J.A., Payne, C.E. (2012) Ultra-precise stable Fe isotope measurements by high resolution multiple-collector inductively coupled plasma mass spectrometry with a 57Fe- 58Fe double spike. *Chemical Geology* 304–305, 18–25.

Oakley, A. (2008) A multi-channel seismic and bathymeric investigation of the central Mariana convergent margin [Ph.D. dissertation]. University of Hawaii. http://www.soest.hawaii.edu/GG/resources/theses/Oakley Dissertation 2008.pdf

Oakley, A.J., Taylor, B., Fryer, P., Moore, G.F., Goodliffe, A.M., Morgan, J.K. (2007) Emplacement, growth, and gravitational deformation of serpentinite seamounts on the Mariana forearc. *Geophysical Journal International* 170, 615–634.

Oakley, A.J., Taylor, B., Moore, G.F. (2008) Pacific plate subduction beneath the central Mariana and Izu-Bonin fore arcs: new insights from an old margin. *Geochemistry, Geophysics, Geosystems* 9, Q06003.

Sossi, P.A., Halverson, G.P., Nebel, O., Eggins, S.M. (2015) Combined separation of Cu, Fe and Zn from rock matrices and improved analytical protocols for stable isotope determination. *Geostandards and Geoanalytical Research* 39, 129–149.

Weyer, S., Ionov, D.A. (2007) Partial melting and melt percolation in the mantle: The message from Fe isotopes. *Earth and Planetary Science Letters* 259, 119–133.

Williams, H.M., Bizimis, M. (2014) Iron isotope tracing of mantle heterogeneity within the source regions of oceanic basalts. *Earth and Planetary Science Letters* 404, 396–407.